Alignment of axial anisotropy of a mononuclear hexa-coordinated Co(II) complex in lattice shows improved single molecule magnet behavior over a 2D coordination polymer having similar ligand field

Ajit Kumar Kharwar, Arpan Mondal and Sanjit Konar

Department of Chemistry, Indian Institute of Science Education and Research Bhopal, Bhopal Bypass road, Bhauri, Bhopal-462066, MP, India.

Table S1. Crystal data and structure refinement for complexes **1** and **2**

Identification code	**1**	2016192
Empirical formula	$C_{23}H_{20}Co_{0.5}N_5O_2S$	$C_{46}H_{42}CoN_{14}OS_2$
Formula weight	459.96	929.98
Temperature/K	140.0	140.0
Crystal system	triclinic	monoclinic
Space group	P-1	$P2_1/c$
a/Å	8.3970(4)	20.7532(14)
b/Å	8.8505(5)	11.7938(10)
c/Å	14.8758(8)	19.5101(14)
α/°	85.880(2)	90
β/°	86.441(2)	109.048(2)
γ/°	74.570(2)	90
Volume/Å^3	1061.87(10)	4513.8(6)
Z	2	4
ρ_{calc}g/cm^3	1.439	1.368
μ/mm^{-1}	0.561	0.526
F(000)	477.0	1932.0
Crystal size/mm^3	0.92 × 0.71 × 0.56	0.72 × 0.61 × 0.47
Radiation	MoKα (λ = 0.71073)	MoKα (λ = 0.71073)
2Θ range for data collection/°	4.782 to 57.574	4.91 to 50.216
Index ranges	-11 ≤ h ≤ 11, -11 ≤ k ≤ 11, -20 ≤ l ≤ 20	-24 ≤ h ≤ 24, -14 ≤ k ≤ 14, -23 ≤ l ≤ 22
Reflections collected	39242	37628
Independent reflections	5526 [R_{int} = 0.0415, R_{sigma} = 0.0262]	7995 [R_{int} = 0.0691, R_{sigma} = 0.0579]
Data/restraints/parameters	5526/0/288	7995/0/594
Goodness-of-fit on F^2	1.039	1.130
Final R indexes [I>=2σ (I)]	R_1 = 0.0319, wR_2 = 0.0687	R_1 = 0.0607, wR_2 = 0.1198
Final R indexes [all data]	R_1 = 0.0417, wR_2 = 0.0727	R_1 = 0.0900, wR_2 = 0.1300
Largest diff. peak/hole / e Å^{-3}	0.32/-0.36	0.70/-0.57

[a]$R_1 = \Sigma||Fo| - |Fc||/\Sigma|Fo|$. [b]$wR_2 = [\Sigma w(Fo^2 - Fc^2)/(Fo^2)^2]^{1/2}$

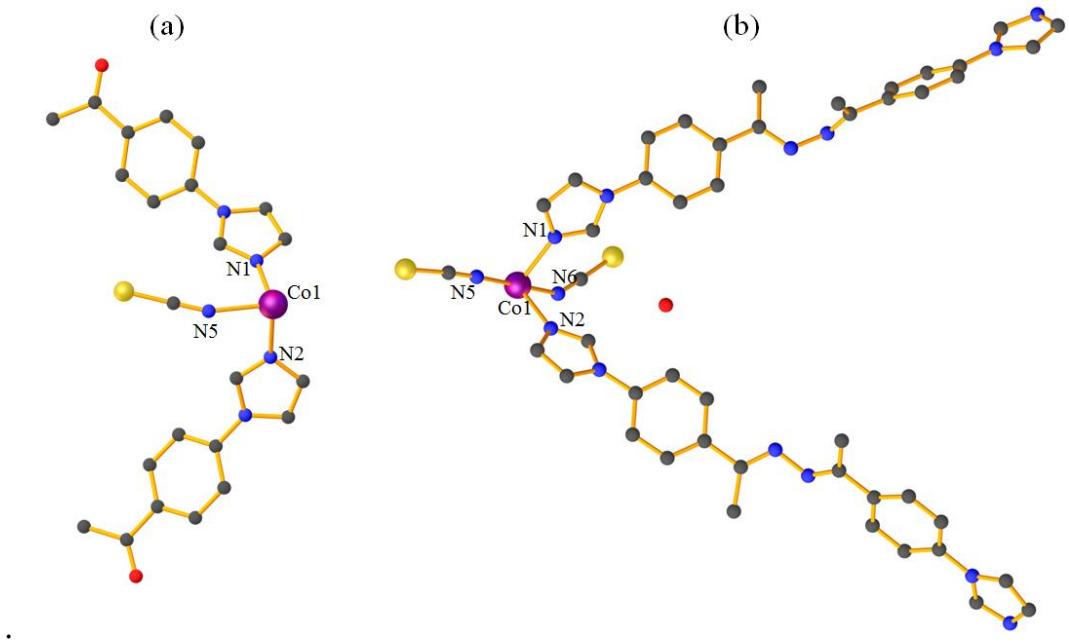

Figure S1. Asymmetric unit of complexes **1** and (b) **2**. Colour code C, gray; N, blue; O, red; Co, purple; S, yellow.

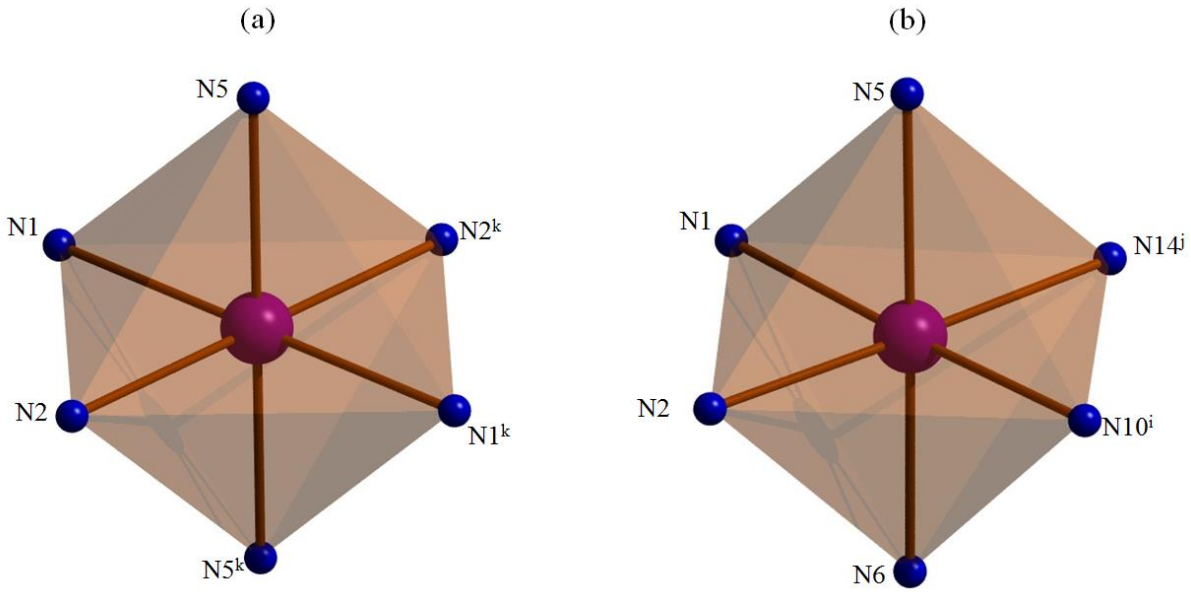

Figure S2. (a) Distorted octahedral coordination geometry around the Co^{II} in **1** and (b) **2.** Colour code N, blue; Co, purple. (i = 2-x, -3/2+y, 3/2-z, j = 1-x, -3/2+y, 1/2-z, k = 1-x, 2-y, 1-z).

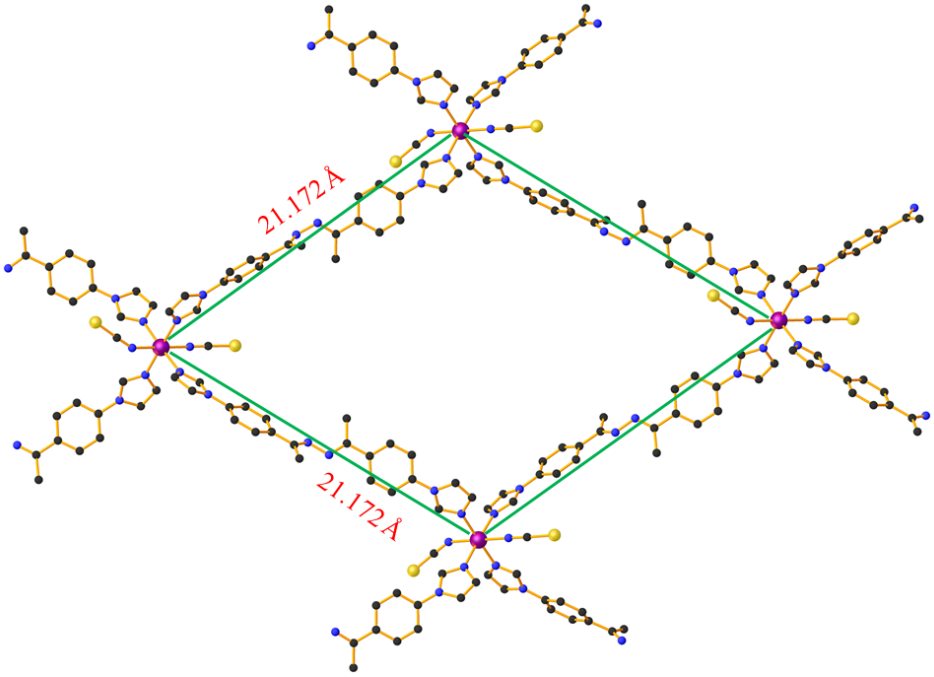

Figure S3. [4+4] metallocyclic unit formed in complex **2**.

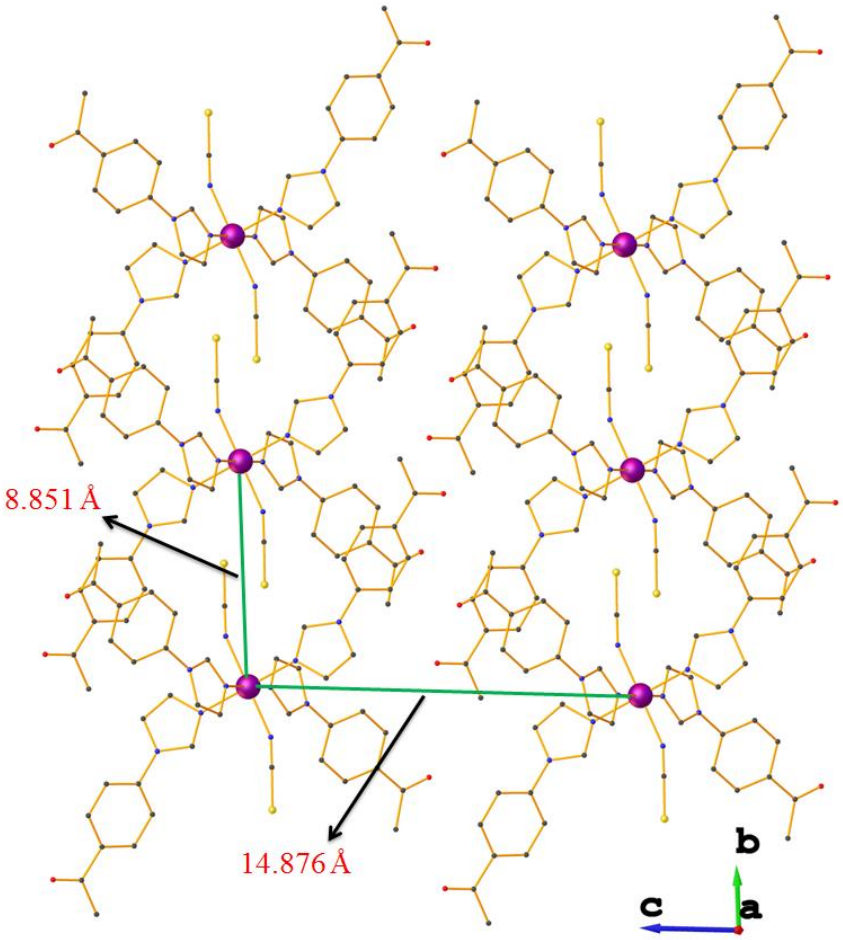

Figure S4. Distance between the Co^{II} centres in 3D packed structure of complex **1**.

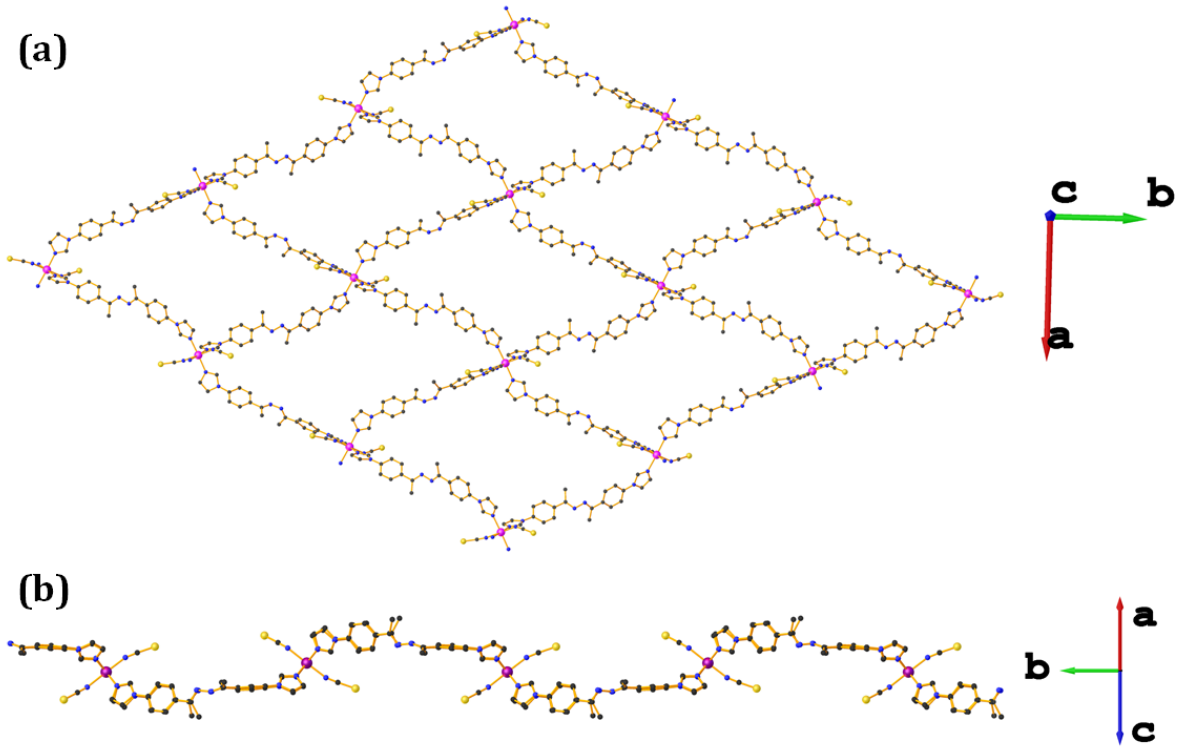

Figure S5. (a) Extended 2D sheet of complex **2** along *ab* plane and (b) along b axis.

Table S2. Bond distances (Å) around Co^{II} centres in complexes **1** and **2**

Complex 1		**Complex 2**	
Co1N1	2.164(11)	Co1N1	2.123(3)
$Co1N1^{k}$	2.164(11)	Co1N2	2.143(3)
Co1N2	2.129(11)	Co1N5	2.122(3)
$Co1N2^{k}$	2.129(11)	Co1N6	2.139(3)
Co1N5	2.132(11)	$Co1N10^{i}$	2.163(3)
$Co1N5^{k}$	2.132(11)	$Co1N14^{j}$	2.148(3)

i = 2-x, -3/2+y, 3/2-z, j = 1-x, -3/2+y, 1/2-z, k = 1-x, 2-y, 1-z

Table S3. Bond angles (°) around Co^{II} centres in **1** and **2**

Complex 1		**Complex 2**	
N5Co1N5^{k}	180.0	N1Co1N2	91.5(11)
N2^{k}Co1N1^{k}	93.90(4)	N1Co1N10^{i}	91.25(12)
N2^{k}Co1N1	86.10(4)	N1Co1N14^{j}	177.71(12)
N2Co1N1^{k}	86.10(4)	N1Co1N6	89.84(12)
N2Co1N1	93.90(4)	N2Co1N10^{i}	177.14(12)
N2Co1N5	88.65(4)	N2CoN14^{j}	90.62(12)
N2^{k}Co1N5^{k}	88.65(4)	N5Co1N1	90.94(12)
N2^{k}Co1N5	91.35(4)	N5Co1N2	90.59(12)
N2Co1N5^{k}	91.35(4)	N5Co1N10^{i}	88.61(12)
N1Co1N1^{k}	180.0	N5Co1N14^{j}	89.90(12)
N5^{k}Co1N1	89.17(4)	N5Co1N6	178.91(13)
N5Co1N1^{k}	89.17(4)	N14^{j}Co1N10^{i}	86.64(12)
N5^{k}Co1N1^{k}	90.83(4)	N6Co1N2	90.16(12)
N5Co1N1	90.83(4)	N6Co1N10^{i}	90.61(12)
N5Co1N5^{k}	180.00(6)	N6Co1N14^{j}	89.29(12)

i = 2-x, -3/2+y, 3/2-z, j = 1-x, -3/2+y, 1/2-z, k = 1-x, 2-y, 1-z

Table S4. Shape Analysis

HP-6 1 D_{6h} Hexagon

PPY-6 2 C_{5v} Pentagonal pyramid

OC-6 3 O_h Octahedron

TPR-6 4 D_{3h} Trigonal prism

JPPY-6 5 C_{5v} Johnson pentagonal pyramid J2

Structure [ML_6]	HP-6	PPY-6	**OC-6**	TPR-6	JPPY-6
Complex 1	31.742	29.592	**0.099**	16.132	32.992
Complex 2	32.804	29.548	**0.038**	16.129	33.200

Highlighted red colour shows the actual geometry of the metal centre with minimum distortion.

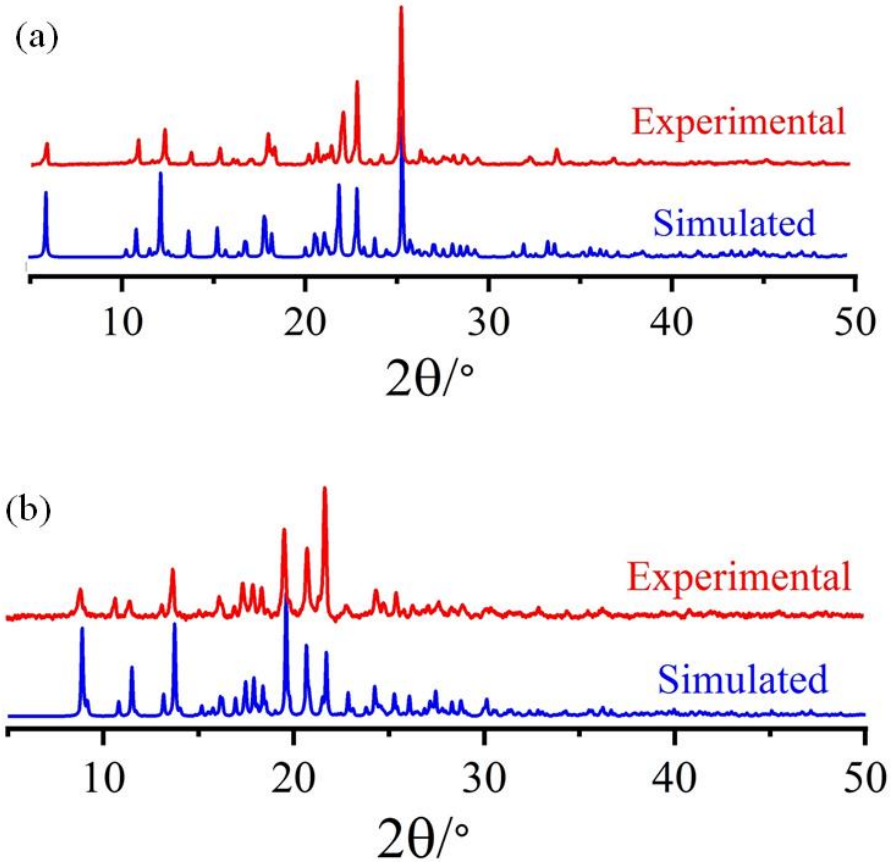

Figure S6. (a) Experimental and simulated PXRD patterns of complexes **1** and (b) **2.**

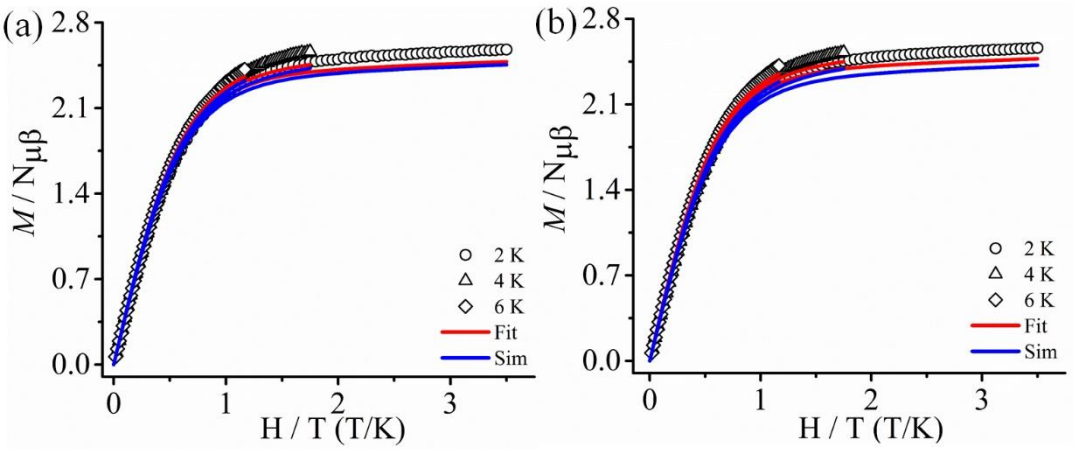

Figure S7. $M/N_{\mu B}$ vs. H/T plots at the indicated temperatures for complexes **1**-**2** (a-b). The red lines are the best fit and blue lines are the best simulation using spin Hamiltonian and T-P isomorphism respectively.

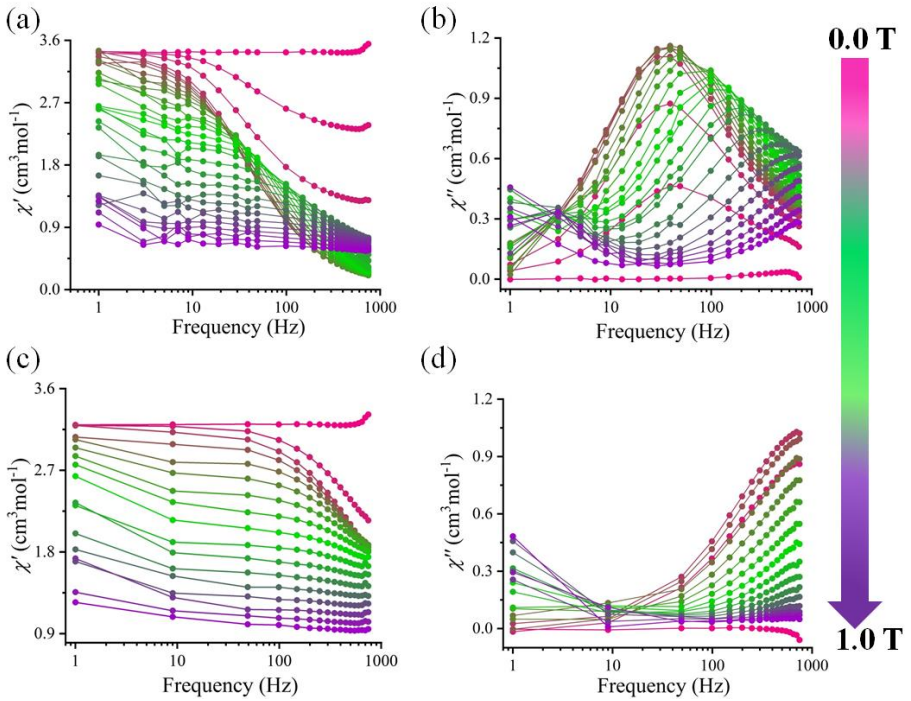

Figure S8. (a) Frequency dependency of the in-phase (χ_M') and (b) out-of-phase (χ_M'') AC magnetic susceptibility plot under different external magnetic fields for complex **1**. (c) Frequency dependency of the in-phase (χ_M') and (d) out-of-phase (χ_M'') AC magnetic susceptibility plot under different external magnetic fields for complex **2**.

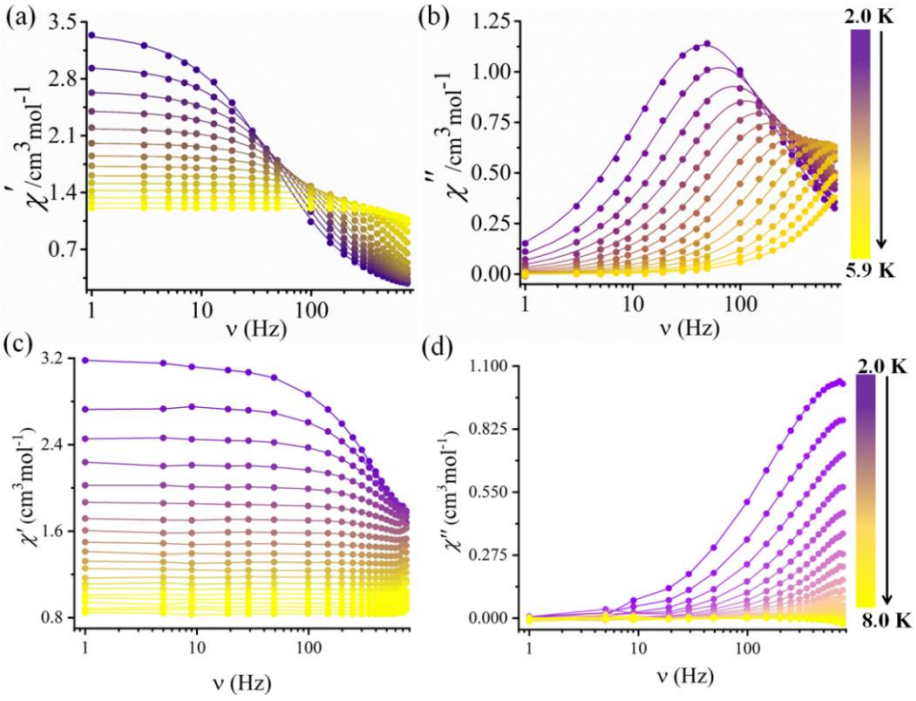

Figure S9. (a) Frequency dependency of the in-phase (χ_M') and (b) out-of-phase (χ_M'') AC magnetic susceptibility plots for complex **1** and (c), (d) for complex **2** under 0.15 T dc field respectively.

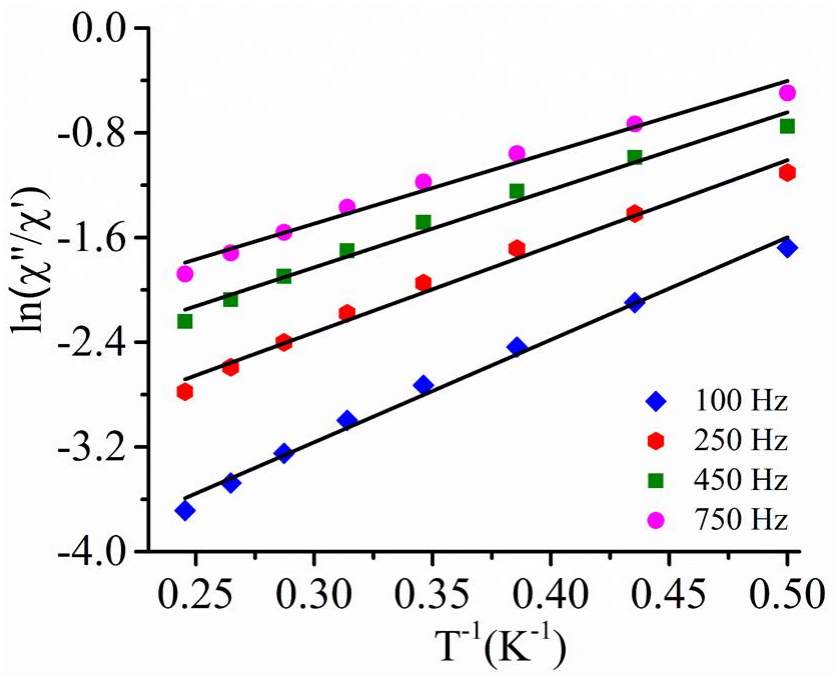

Figure S10. The solid lines represent the best fitting (c) $\ln(\chi_M''/\chi_M')$ *vs* 1/T plot and fitting (solid line) with Debye equation for complex **2**.

Table S5. The parameters obtained from the fitting of frequency dependency data using generalized Debye model for complex **1**

T (K)	χ_T	τ (s)	χ_S	α
2	3.38718	0.00348	0.10393	0.23158
2.3	2.97056	0.00249	0.10452	0.21241
2.6	2.6562	0.00185	0.09875	0.20106
2.9	2.41363	0.00141	0.09376	0.19101
3.2	2.19418	0.00109	0.09969	0.17325
3.5	2.01235	8.42788E-4	0.10137	0.15585
3.8	1.8542	6.45135E-4	0.09363	0.13642
4.1	1.72225	4.93526E-4	0.09425	0.11408
4.4	1.60677	3.70565E-4	0.08977	0.08958
4.7	1.51182	2.70985E-4	0.06704	0.07361
5	1.42408	1.91639E-4	0.01779	0.06065
5.3	1.33657	1.4582E-4	0.05883	0.01893
5.6	1.26919	1.01291E-4	0	0.01247
5.9	1.20852	7.46636E-5	0	0.01034

Table S6. ORCA/CASSCF, ORCA/CASSCF+NEVPT2 computed *D*, |*E*| and g_{iso} values for the complexes **1**-**2**. (a = ORCA/CASSCF/NEVPT2)

Complex	D_{expt} (cm^{-1})	D_{cal}(cm^{-1})	E_{exp} (cm^{-1})	E_{cal} (cm^{-1})	Exp. (g_x, g_y, g_z)	g_{cal}
1	+84.16	+118.20	0.07(2)	11.82	2.28, 2.28, 2.21	2.35
2	+89.30	+135.06	0.08(3)	6.34	2.30, 2.30, 2.18	2.30

Table S7. NEVPT2 calculated transition energy and their contribution to *D*, *E* for complexes **1** and **2**

Complex **1**				Complex **2**			
Excited state	Energy (cm^{-1})	Cont. D (cm^{-1})	Cont. E (cm^{-1})	Excited state	Energy (cm^{-1})	Cont. D (cm^{-1})	Cont. E (cm^{-1})
1	315.9	53.306	52.356	1	223.2	56.467	55.728
2	560.5	39.635	-38.060	2	375.2	48.964	-47.777
3	8325.6	-0.421	0.975	3	8129.0	2.617	0.275
4	9461.8	0.968	-0.150	4	9141.9	2.211	-1.491
5	9501.7	4.331	-1.720	5	9661.2	3.458	0.730

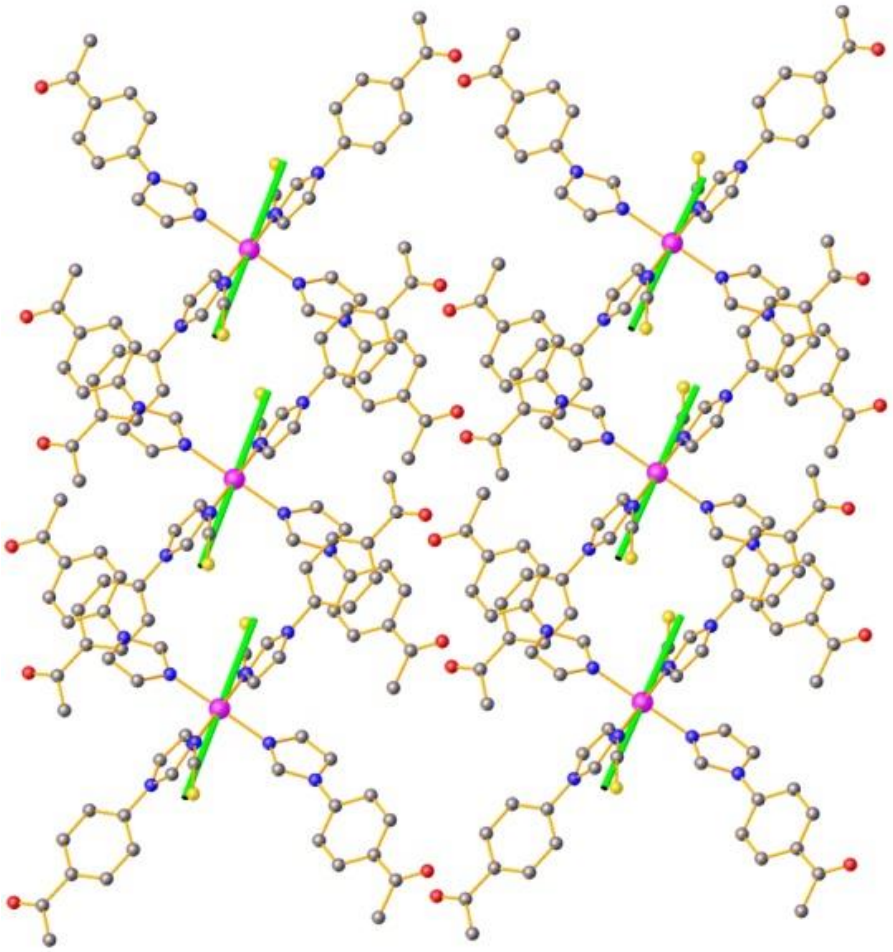

Figure S11. Orientation of ground state anisotropy axis in 3D packed structure of **1**.